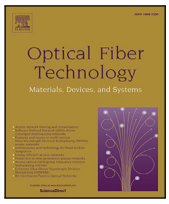
Optical Fiber Technology 100 (2026) 104666



Contents lists available at ScienceDirect

Optical Fiber Technology

journal homepage: www.elsevier.com/locate/yofte



Regular Articles



Inter-core crosstalk analysis of homogeneous 12-core weakly-coupled multi-core fiber layouts for short-reach bidirectional transmission

Tomás I. Martins [a], João L. Rebola [a,b,*], Adolfo V.T. Cartaxo [a,b]

[a] Iscte - Instituto Universitário de Lisboa, Lisbon, Portugal
[b] Optical Communications and Photonics Group, Instituto de Telecomunicações, Lisbon, Portugal

ARTICLE INFO

Keywords:
Bidirectional transmission
Inter-core crosstalk
Multi-core fibers
Optical short-reach links
Space division multiplexing

ABSTRACT

The feasibility of 12-core layouts of standard cladding diameter homogeneous single-mode weakly-coupled multi-core fibers with bidirectional transmission is assessed, regarding the inter-core crosstalk (ICXT) level in bidirectional transmission short-reach links. Four layouts reported in the literature, namely the square, hexagonal, outer circle and inner square and the reference layout, are compared. The square layout is the best for bidirectional transmission with propagation-direction interleaving in the C-band, with a reduction of more than 18 dB in the total ICXT level when compared to unidirectional transmission, for fiber lengths up to 10 km. This square layout has an outer cladding thickness of 22.5 μm, a core pitch of 25.3 μm, and a low confinement loss of 0.0045 dB/km due to suitable choice of the core parameters. Achieving a bidirectional ICXT level of -47.8 dB and -34 dB at 1 km and 10 km, respectively, the square layout reaches the maximum allowable ICXT level, for an outage probability of 10^{-4} with 4-level pulse amplitude modulation intensity-modulation and direct-detection systems, of -23.6 dB at 37 km (a 35 km longer length than the one found in unidirectional transmission with the same layout).

1. Introduction

Nowadays, Internet usage is in constant growth. In 2023, 5.4 billion people had access to the internet, representing an increase of 4.7% from previous year [1]. With the adoption of internet of things, the steer towards the broader use of content streaming, cloud computing and the emergence of massive artificial intelligence (AI) applications, an ever-growing demand for an increase in data capacity in telecommunication networks exists [2].

Currently, most global telecommunication networks are supported by the optical fiber infrastructure [2], using wavelength division multiplexing (WDM) transmission over standard single-core single-mode fibers (SMFs). However this transmission technique is approaching its predicted maximum capacity of 100 Tb/s within a single fiber [3,4]. To overcome this bottleneck, space division multiplexing (SDM) solutions propose the use of multiple spatial paths in an optical fiber link, by resorting to specialty fibers, such as few-mode fibers, multi-mode fibers and multi-core fibers (MCF), or even to using bundles of parallel single-core SMFs [5].

MCF are fibers that have more than one core inside the same cladding [6]. If all cores in the fiber are designed to have the same physical characteristics, the fiber is called a homogeneous MCF. By having cores with different physical properties inside the same cladding, an heterogeneous MCF, it is possible to decrease ICXT and therefore place cores more closely packed when compared to a homogeneous MCF with the same cladding diameter (CD) [7]. However, homogeneous MCFs offer a simpler migration path from currently installed systems [8,9]. Furthermore, even when designed to be homogeneous, some degree of heterogeneity will be introduced in the MCF during manufacturing [9,10].

MCFs can be classified according to their inter-core coupling strength in two main categories: strongly-coupled MCFs (SC-MCFs) and weakly-coupled MCFs (WC-MCFs) [3]. SC-MCFs are fibers designed with a core pitch short enough to allow for significant signal coupling between cores. At the receiving end, the coupled modes must be separated with the use of sophisticated multiple-input multiple-output (MIMO) digital signal processing (DSP) [3,6]. SC-MCFs have been reported as good candidates for long-haul transmission scenarios [11], where complex and costly receivers are justifiable. WC-MCFs are designed with the distance between cores large enough to reduce inter-core mode coupling. Although their design, the small power leakage between nearest cores, known as inter-core crosstalk (ICXT), may still limit their transmission performance [3]. In WC-MCFs, each core can be handled as an independent transmission channel, being

* Corresponding author at: Iscte - Instituto Universitário de Lisboa, Lisbon, Portugal.
E-mail address: joao.rebola@iscte-iul.pt (J. Rebola).

https://doi.org/10.1016/j.yofte.2026.104666
Received 25 February 2026; Received in revised form 21 April 2026; Accepted 25 April 2026
Available online 2 May 2026
1068-5200/© 2026 The Authors. Published by Elsevier Inc. This is an open access article under the CC BY license (http://creativecommons.org/licenses/by/4.0/).

this type of fiber more compatible with existing single-core SMF-based networks, as the same SMF transceivers can be used without needing MIMO DSP at the receiver [6,12]. Accommodating in the cladding the highest number of cores maximizes the data throughput [13].

For cost-sensitive scenarios, such as the case of short-reach links, mainly intra-datacenter and some inter-datacenter links, with distances that can reach 2 km and 100 km, respectively, WC-MCFs possess a competitive advantage over SC-MCFs [11]. For such optical links, when employing intensity-modulation and direct detection to keep the complexity low, 4-level pulse amplitude modulation (PAM-4) has been used with the goal of improving data capacity from the previously used on–off keying modulation [14]. With PAM-4, the maximum allowed ICXT level in the link to achieve an outage probability lower than 10^{-4} is −23.3 dB [15]. Additionally, for higher compatibility, WC-MCFs should also have a standard CD of 125 μm, like the single-core SMFs currently used in these scenarios.

Nowadays the deployment of WC-MCFs is in its initial phase, with several test beds installed around the world, such as in Fujimino, Japan [16], Guangzhou, China [17], the INCIPICT project in L'Aquila, Italy [18], and LUMIRing in Lisbon, Portugal [19]. Regarding commercial use, in 2023, Google started to deploy fibers with two cores, in the Taiwan-Philippines-US trans-pacific cable [20]. WC-MCFs with four cores [21,22] and eight cores [23,24] within a standard CD have been designed and fabricated, being the latter the WC-MCFs with the highest number of cores currently proposed and fabricated for telecommunications. Some of these higher core-count WC-MCFs were designed and are suitable for bidirectional transmission with propagation-direction interleaving (PDI) [25–28], a technique consisting of attributing opposite directions of signal propagation to adjacent cores to reduce the amount of co-propagating cores that neighbor each other. This technique allows for full duplex transmission with one single WC-MCF whilst simultaneously and significantly reducing ICXT [25].

In this work, we assess and compare various layouts for homogeneous 12-core WC-MCFs with standard CD for short-reach optical links, regarding their geometrical properties and ICXT level in bidirectional transmission with the use of PDI in the C-band, where the maturity and efficiency of wavelength division multiplexing technology allows for proportional efficiency in bidirectional bandwidth [29].

The reminder of this paper is organized as follows. In Section 2, the structure of WC-MCFs is presented and the refractive index profile of trench-assisted (TA) fibers is described with detail. Then, design considerations for the 12-core WC-MCFs are discussed, the analytical expressions required to obtain the different contributions of ICXT level are presented and the design choice for the core structure parameters is explained. In Section 3, four 12-core MCF layouts proposed in the literature are presented and compared and the geometric characteristics of these layouts are evaluated. In Section 4, the ICXT level of the 12-core WC-MCFs with different layouts is assessed, focusing on bidirectional transmission with PDI in short-reach links. The last section summarizes the main conclusions of this work.

2. WC-MCF parameters

In this section, the structure of WC-MCFs with TA refractive index profile is presented and the main parameters are described. Then, the design considerations employed for obtaining a WC-MCF with a core-count of twelve are discussed. Lastly, the core structure parameters are presented and their choice is explained.

2.1. Structure of WC-MCFs

When compared to single-core SMFs, MCFs have additional parameters that must be designed, such as the number of cores, the placement of the cores, if the cores are homogeneous or heterogeneous, the distance between cores, known as core pitch (Λ) and the distance between the center of the closest core to the cladding–coating interface, d_{oct}, also known as outer cladding thickness (OCT) [6,30]. These characteristics are indicated in Fig. 1, which shows a schematic of a four-core MCF cross-section, where we are assuming that all cores have the same characteristics (homogeneous cores), an assumption that is followed throughout this work. The distance corresponding to the CD, d_{cd} is also represented in Fig. 1. In MCFs, the balance between the core pitch and the OCT must be considered carefully. Placing the cores closer to the coating–cladding interface leads to an increase in power leakage from the cores to the coating, an effect known as confinement loss (CL) [3]. However, it allows for a higher cladding-area to place the cores, hence allowing the reduction of the ICXT level due to the cores proximity or to increase the number of cores inside the cladding to achieve an enhanced capacity [27].

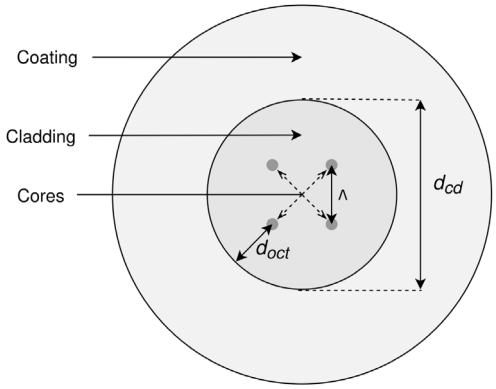


Fig. 1. Schematic of a four-core MCF cross-section.

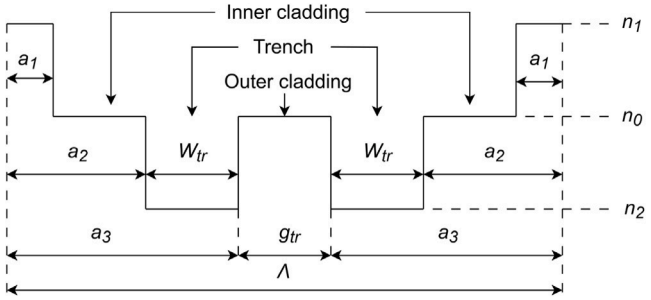


Fig. 2. Representation of the TA refractive index profile between the center of two adjacent cores.

To achieve a strong power confinement within the cores, a TA refractive index profile is usually employed [12,22]. In this profile, a trench composed of a material with a lower refractive index is placed between the inner and outer claddings, surrounding the core [3]. Fig. 2 shows a representation of the TA refractive index profile between the center of two adjacent cores. On the vertical axis, n_0, n_1 and n_2 are the refractive index of the cladding, core and trench, respectively, with n_1 and n_2 obtained by:

$$n_x = (1 + \Delta_x)n_0 \tag{1}$$

where Δ_x is the relative refractive index difference between core and cladding for $x = 1$, and the relative refractive index difference between trench and cladding for $x = 2$. On the horizontal axis, a_1, a_2 and W_{tr} represent the core radius, the distance from the center of the core to the inner edge of the trench and the width of the trench, respectively. By adding the distance from the center of the core to the inner edge of the trench and the width of the trench, we obtain the total radius of the core structure, defined as a_3. The distance between trenches in two adjacent cores is defined as g_{tr}.

2.2. Design considerations

The objective of the MCF design in this work is to have a fiber with a core-count of twelve within the standard CD, that operates in the C-band leading to a total ICXT level lower than −23.3 dB per link. Furthermore, the MCF must also have a CL lower than 0.01 dB/km, a value that has been established in several studies as the upper limit for CL, deeming it acceptable for short-reach optical links [10,12,22,23].

To calculate the ICXT level, the power coupling coefficient of the interfered core n and interfering core m is obtained with [3]:

$$h_{nm} = 2\frac{\kappa_{nm}^2 R_b}{\beta \Lambda} \tag{2}$$

where R_b is the bending radius, κ_{nm} is the mode coupling coefficient between two cores n and m, calculated using equation (5) of [31] and β is the propagation constant, calculated using equations (7) and (11) of [32].

In unidirectional transmission, as all cores propagate in the same direction, the total ICXT power originated in core n by core m has two contributions, the direct ICXT power and the indirect ICXT power, given, respectively, by [23,30,31]:

$$ICXT_{dir,nm} = h_{nm} L \tag{3}$$

$$ICXT_{indir,nmp} = \frac{h_{nm} h_{mp} L^2}{2} \tag{4}$$

where L is the fiber length and h_{mp} represents the power coupling coefficient between cores m and p.

By employing bidirectional transmission, we have cores that co-propagate and cores that counter-propagate, giving rise to more non-negligible ICXT contributions: Rayleigh backscattered ICXT and back reflected ICXT [25,33]. With the use of PDI, where signals propagate with opposite directions in adjacent cores, and if the MCF layout is properly designed, the direct ICXT can be neglected, and indirect, Rayleigh backscattered and back-reflected ICXTs gain relevance and pose significant contributions to the total ICXT level. However, this may not be the case where the core layout does not allow the implementation of PDI in all cores. So, to determine properly the ICXT level in WC-MCFs with bidirectional transmission with the use of PDI, all four ICXT contributions must be taken into account. The Rayleigh backscattered ICXT power and the back reflected ICXT power levels are given, respectively, by [25,33,34]:

$$\begin{aligned} ICXT_{bs,nm} = h_{nm} L S \frac{\alpha_R}{\alpha} \cdot \left\{ \frac{\sinh(\alpha L)}{\alpha L + 2h_{nm} L} - \frac{\alpha L}{\alpha L + 2h_{nm} L} \right. \\ \left. \cdot \left[\frac{1 - \exp(-4h_{nm} L)}{4h_{nm} L} \right] \exp(-\alpha L) \right\} \cdot \frac{2}{1 + \exp(2h_{nm} L)} \end{aligned} \tag{5}$$

$$ICXT_{ref} = 2h_{nm} L R_{trx} \exp(-\alpha L), \tag{6}$$

where S is the recapture factor of the Rayleigh scattering component into the backward direction, α_R is the attenuation coefficient due to the Rayleigh scattering, α is the core attenuation coefficient and R_{trx} is the reflection at the transceiver.

To accurately estimate the mean ICXT power of the layouts analytically, the ICXT level between every core pair has to be calculated. The total direct ICXT level that affects core n, using Eq. (3) and accounting for all cores that co-propagate with core n, can be obtained with:

$$ICXT_{total,dir,n} = \sum_{\substack{m \in D(n) \\ m \neq n}} ICXT_{dir,nm}, \tag{7}$$

where $D(n)$ represents the set of cores that have the same direction of signal propagation as core n.

For the indirect ICXT level that affects core n, the same procedure is done with Eq. (4), but only taking into account cores that are second adjacent to core n:

$$ICXT_{total,indir,n} = \sum_{m \in N(n)} \sum_{p \in N(m)} ICXT_{indir,nmp} \tag{8}$$

Table 1
Core structure parameters of Core 1, taken from [24].

Parameter	Core 1
a_1 [μm]	4.12
a_2 [μm]	6.16
W_{tr} [μm]	4.87
Δ_1 [%]	0.52
Δ_2 [%]	−0.7

where $N(x)$ represents the set of cores that are adjacent to core x, with $x = n$ or $x = m$. In the case of the Rayleigh-backscattered ICXT and back-reflected ICXT, only the cores with opposite direction of signal propagation to core n contribute to these ICXT types. As such, the Rayleigh backscattered ICXT level in core n can be obtained with:

$$ICXT_{total,bs,n} = \sum_{m \in O(n)} ICXT_{bs,nm}, \tag{9}$$

where $O(x)$ represents the set of cores that have an opposite direction of signal propagation to core x. Similarly, the back-reflected ICXT level in core n is obtained with:

$$ICXT_{total,ref,n} = \sum_{m \in O(n)} ICXT_{ref,nm}. \tag{10}$$

As such, the total ICXT level in unidirectional transmission in core n is given by:

$$ICXT_{uni,n} = ICXT_{total,dir,n} + ICXT_{total,indir,n}, \tag{11}$$

and the total ICXT level in bidirectional transmission is given by:

$$\begin{aligned} ICXT_{bi,n} = & ICXT_{total,dir,n} + ICXT_{total,indir,n} \\ & + ICXT_{total,bs,n} + ICXT_{total,ref,n}. \end{aligned} \tag{12}$$

2.3. Core structure parameters

We use the core parameters detailed in Table 1, which are equal to the parameters of core 1 presented in [24]. In that study, the authors implemented an AI-based method to design the core parameters of a TA-profile with the intent of optimizing the CL of the core in the C-band. By doing so, the authors designed a core with a CL of 0.0045 dB/km for an OCT of 22.5 μm and a CL of 3.6×10^{-5} dB/km for an OCT of 28 μm. To reach this CL, the core has been proposed with a core structure diameter of 22.06 μm, strong power confinement due to high refractive index differences between trench, cladding and core, and an effective area of 54.26 μm^2. All these properties are desirable for the design of a 12-core fiber with standard CD. Furthermore, the demonstrated feasibility of fabricating a MCF with these core parameters [24] indicates that such a MCF is unlikely to present significant challenges during manufacturing, even for a 12-core MCF.

3. 12-Core MCF layouts

In this section, a discussion on the 12-core MCF layouts already proposed in the literature is provided.

3.1. Layouts reported in the literature

In the literature, the squared layout is the most common layout considered for 12-core MCFs [35,36]. Other layouts reported in the literature are the hexagonal layout [37] and the outer circle and one inner square layout [38]. By applying the solution of packing circles in circles, detailed in [39], to the layout of a MCF, it is possible to obtain what has been reported as the best layout for ICXT mitigation in unidirectional transmission with twelve cores [13]. The layouts reported in the literature and considered in this work are represented in Fig. 3, with standard CD and an OCT of 22.5 μm, where the two different colors of the cores represent different directions of signal

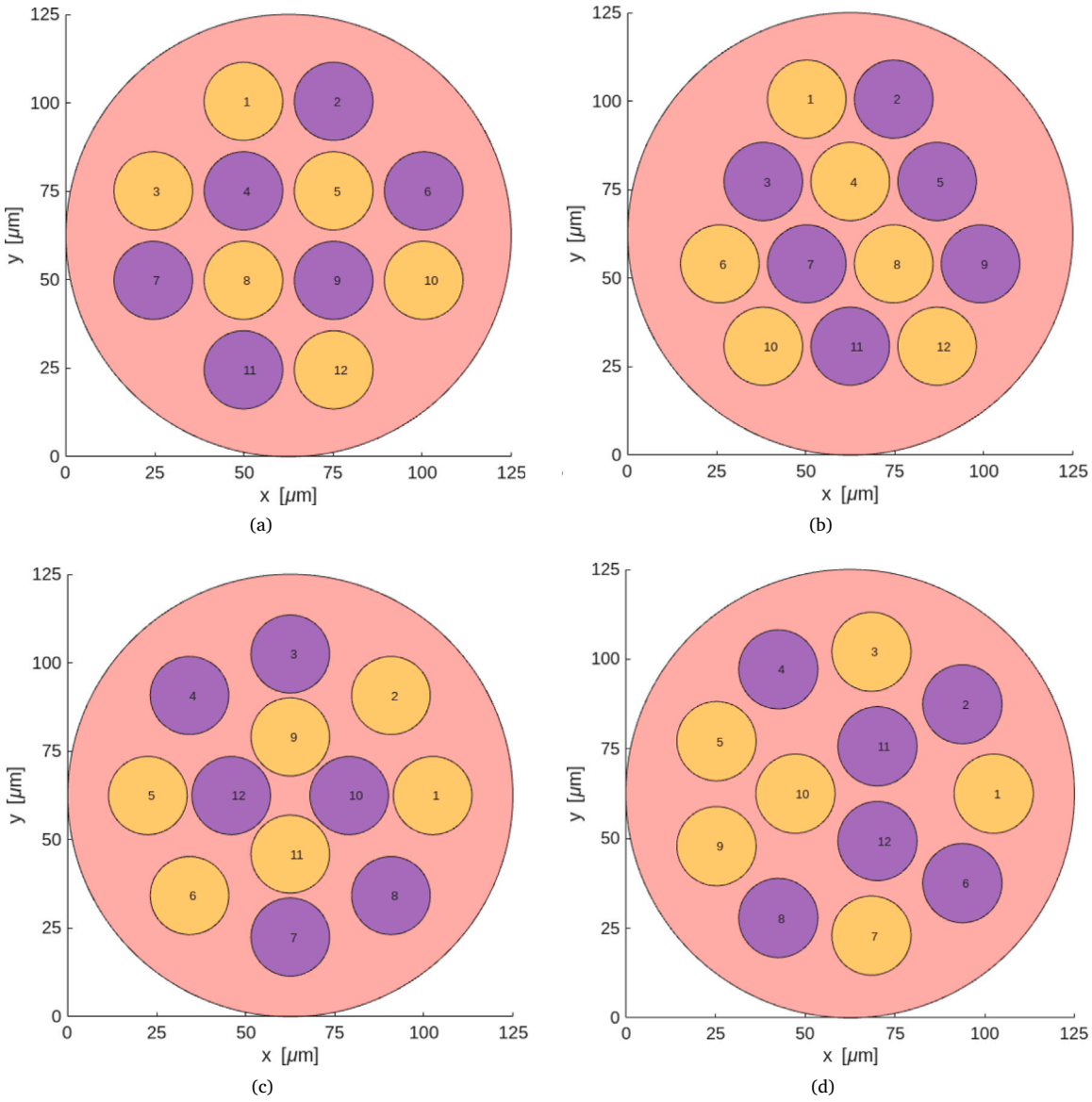


Fig. 3. Schematic of 12-core standard CD WC-MCFs with a (a) square layout [35,36], (b) modified hexagonal layout based on [37], (c) one outer circle and one inner square layout [38] and (d) reference layout [13,39]. The different colors of the cores correspond to two opposite directions of signal propagation, assigned to maximize the benefits attained from bidirectional transmission with PDI.

propagation, and are assigned with the intent of minimizing the number of adjacent cores with the same direction of signal propagation. This is important because, in bidirectional transmission with the use of PDI, adjacent cores should not have the same direction of propagation, to reduce direct ICXT.

In Fig. 3(a), a MCF with the square layout is shown. In this layout, the adjacent cores are all equidistant. The cores in the central square have four adjacent cores, whilst the outer cores only have two adjacent cores. Due to the directions of signal propagation assigned, no core has an adjacent core transmitting a signal in the same direction.

Fig. 3(b) represents a MCF with the modified hexagonal layout, where the cores are placed along 4 diagonal lines, with the cores in each line sharing the same direction of propagation and adjacent lines having opposite directions. In the modified hexagonal layout, the core pitch between cores in the same horizontal line is smaller than the core pitch between adjacent cores in the diagonal lines. This ensures that the closest cores are always counter propagating.

The one outer circle and one inner square layout is represented in Fig. 3(c). As the name suggests, in this layout, eight cores are equidistantly placed over a circumference with radius $d_{cd}/2 - d_{oct}$, and the remaining four cores are placed inside that circumference, aligning with the vertical and horizontal axis. For this layout, the assignment of propagation direction is first performed on the cores in the inner square, followed by the cores that are adjacent to those. Lastly, the remaining four cores in the outer circle are assigned directions in a way that each core in the outer circle has only one adjacent outer circle core with the same propagation direction.

By using the solution of packing circles in circles, the MCF layout presented in Fig. 3(d) can be obtained. This layout is considered the best for ICXT suppression in unidirectional transmission, as it is the layout that presents the cores the furthest apart from each other [13], and thus we will refer to it as the reference layout. However, when taking into account bidirectional transmission, it is not possible to attribute opposite directions of signal propagation to all adjacent cores, as there are several cores that contain pairs of adjacent cores that are also adjacent themselves, like between cores 10, 11 and 12. As such, this layout does not allow for PDI in all adjacent core pairs, but some ICXT level suppression can still occur [28].

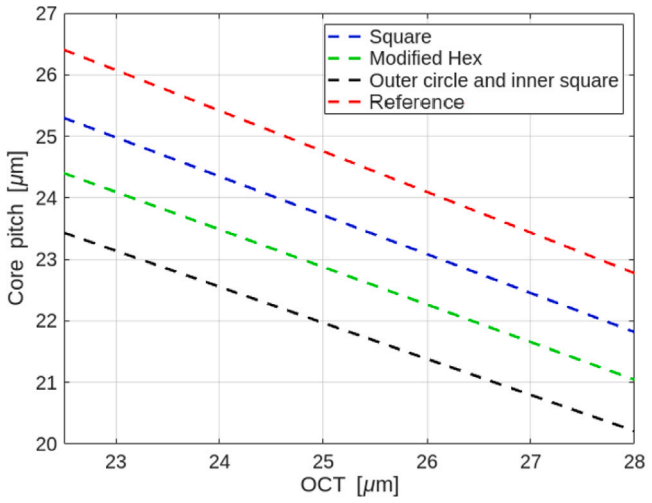


Fig. 4. Core pitch as a function of the OCT for the layouts presented in Fig. 3, using the core parameters shown in Table 1.

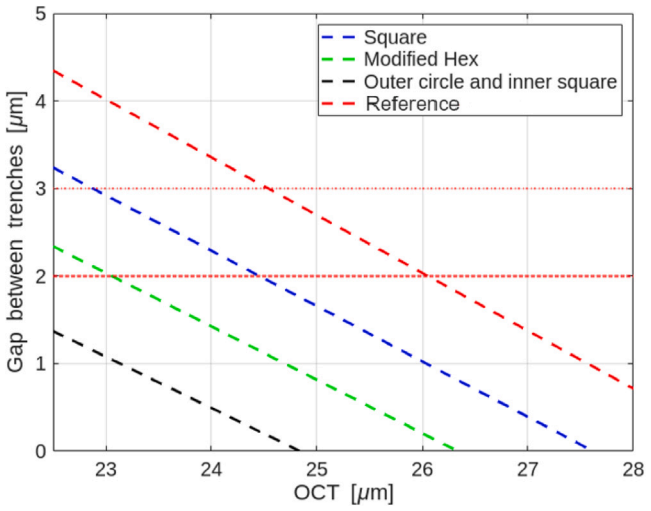


Fig. 5. Gap between trenches as a function of the OCT, for the layouts presented in Fig. 3, using the core parameters shown in Table 1. The horizontal red dotted lines indicate the two limits for the gap between trenches found in the literature.

3.2. Geometric analysis of the 12-core layouts

By combining the MCF layouts presented in Section 3.1 with the core parameters detailed in Table 1, we can obtain the core pitch and gap between the trenches of adjacent cores as a function of the OCT, as shown in Figs. 4 and 5.

For the 12-core square layout, where the distance between cores is equal between all pairs of adjacent cores, the core pitch can be obtained with [40]:

$$\Lambda_{sqr} = \frac{d_{cd} - 2 \cdot d_{oct}}{\sqrt{10}}, \tag{13}$$

which represents the distance from any core to its closest cores. For the modified hexagonal layout, the core pitch can be obtained with:

$$\Lambda_{hex} = (d_{cd} - 2 \cdot d_{oct}) \cdot \sin\left(\frac{\theta}{2}\right), \quad \theta = 0.62 \text{ rad}, \tag{14}$$

which represents the distance from any core to the core immediately to its left or right. For the one outer circle and inner square layout, the core pitch can be obtained by:

$$\Lambda_{sqr_cir} = (2 - \sqrt{2}) \cdot \left(\frac{d_{cd}}{2} - d_{oct}\right), \tag{15}$$

which represents the distance from one of the center cores to any of its adjacent cores. Lastly, for the reference layout, the core pitch can be obtained with:

$$\Lambda_{ref} = (d_{cd} - 2 \cdot d_{oct}) \cdot \sin\left(\frac{\theta}{2}\right), \quad \theta = 0.672 \text{ rad}, \tag{16}$$

which represents the distance from one of the center cores to any of its adjacent cores. With these values, the distance between trenches for layout l can be obtained by:

$$g_{tr,l} = \Lambda_l - 2 \cdot a_3, \tag{17}$$

with $l = sqr, hex, sqr_cir$ or ref.

In Fig. 4, the core pitch between the two closest cores of each layout is presented, for OCTs varying from 22.5 μm and 28 μm, whilst maintaining a standard CD. It is apparent that the reference layout for ICXT suppression in unidirectional transmission has the largest core pitch, 26.4 μm for an OCT of 22.5 μm, which is below the 30 μm core pitch commonly associated with WC-MCFs [33,41,42]. The remaining layouts all have shorter core pitches, with the square layout achieving the second highest core pitch of 25.3 μm at an OCT of 22.5 μm.

The gap between the trenches, obtained with Eq. (17), is shown in Fig. 5, as a function of the OCT. In the literature, it is suggested that this gap should be larger than 2 μm to 3 μm [31,43], as shorter gaps are hard to manufacture. These limits are marked by the horizontal red dotted lines in Fig. 5. Furthermore, for $g_{tr,l} < 0$, the cores physically overlap.

It can be seen from Fig. 5 that only two layouts, the reference layout for ICXT suppression in unidirectional transmission and the square layout, lead to a gap between trenches larger than 3 μm (4.3 μm and 3.2 μm, respectively, for an OCT of 22.5 μm). For this OCT, the modified hexagonal layout presents a gap between trenches of 2.34 μm, failing to meet the most stringent limit, but surpassing the less demanding one. Furthermore, the one outer circle and one inner square layout has the lowest gap between trenches, failing to meet any of the limits considered, with an unfeasible gap of 1.37 μm. Hence, it is excluded from the subsequent analysis performed in this work.

4. ICXT level assessment

In this section, the ICXT level and its main contributions are assessed for unidirectional and bidirectional transmission for the selected 12-core WC-MCF layouts.

4.1. Unidirectional transmission

To understand if there is the need to implement bidirectional transmission to achieve acceptable ICXT levels, we first need to evaluate the ICXT level in unidirectional transmission. For that, it is necessary to identify the most affected core in each layout. As such, Fig. 6 shows the ICXT level in unidirectional transmission for every core of the 12-core (a) square, (b) modified hexagonal and (c) reference layouts, obtained from Eq. (11). In Fig. 6, we discriminate the direct and indirect ICXT contributions, obtained from Eqs. (7) and (8), respectively, for an OCT of 22.5 μm and fiber lengths of 10 km (top row figures) and 100 km (bottom row figures). For this assessment, the wavelength of 1565 nm is considered, as it corresponds to the upper value of the C-band, where the ICXT level is larger.

It can be seen from Fig. 6, that for each layout, the ICXT level is different from core to core. This happens because not every core has the same number of adjacent cores. As expected, for each layout, the cores with the highest level of ICXT correspond to the cores that are closer to the center of the fiber, which have the highest number of adjacent cores.

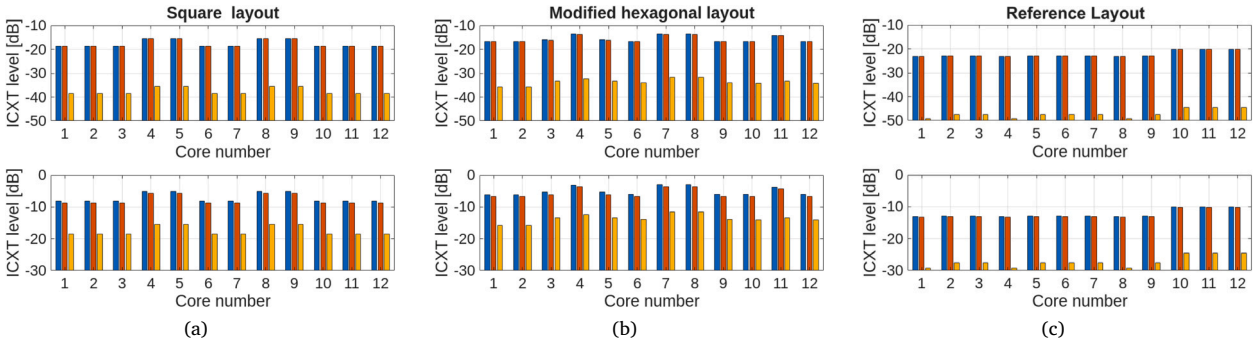


Fig. 6. ICXT level in unidirectional transmission for each core of the (a) square layout, (b) modified hexagonal layout and (c) reference layout for unidirectional transmission. The graphs in the top row are for a fiber length of 10 km, and the bottom row for 100 km. The blue, orange and yellow bars represent the total, direct and indirect ICXT levels, respectively.

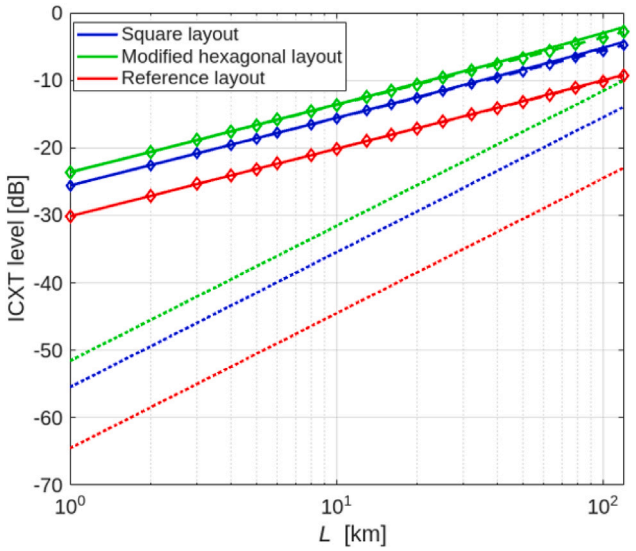


Fig. 7. ICXT level in unidirectional transmission as a function of the fiber length, for the most affected core of the 12-core WC-MCF reference, modified hexagonal and square layouts for a wavelength of 1565 nm. The full, dashed with diamond markers and dotted lines represent the total, direct and indirect ICXT levels, respectively.

For these three layouts, the ICXT level difference between the worst and best cores is 3 dB, as in every layout the most affected core has twice the number of interfering adjacent cores than the least affected core. For the analysis that follows, we will only consider the ICXT of core 4 of the square layout, core 7 of the modified hexagonal layout and core 10 of the reference layout.

Fig. 7 shows the unidirectional ICXT level, including the direct and indirect contributions for the aforementioned cores of the square, modified hexagonal and reference layouts, for a fiber length from 1 km to 120 km. From Fig. 7, it can be seen that, in unidirectional transmission, only the reference layout achieves an ICXT level lower than −30 dB, which happens for the shortest length considered of 1 km. The square layout achieves a unidirectional ICXT level of −25.6 dB at 1 km. From the layouts considered in this section, the modified hexagonal layout is the worst in unidirectional transmission, reaching an ICXT level of −23.6 dB at 1 km. This means that to be within the maximum acceptable ICXT level of −23.3 dB in the link length, with these core parameters, the modified hexagonal, square and reference layout for unidirectional transmission are only suitable for link lengths not exceeding 1 km, 1.5 km and 4 km, respectively. Furthermore, Fig. 7 also shows that, although the indirect ICXT level increases faster with fiber length than the direct ICXT level, for the layouts considered, it only starts making a noticeable contribution to the total ICXT level for distances above 100 km. For shorter lengths, the direct ICXT level is entirely responsible for the ICXT level in the cores.

Table 2
Parameters used for the ICXT level calculation, and their corresponding references.

Parameter	R_b [mm]	$S\frac{\alpha_R}{2\alpha}$ [dB]	R_{irx} [dB]
Value	140	−29.5	−26
Ref.	[23], [24]	[44]	[25]

4.2. Bidirectional transmission

To be able to compare the performance of the 12-core layouts in regard to ICXT level in bidirectional transmission, we have to identify the core most affected by ICXT. To do so, in Fig. 8, the total bidirectional ICXT level of each core of the 12-core (a) square, (b) modified hexagonal and (c) reference layouts, obtained with Eq. (12), as well as the individual ICXT contributions is shown for lengths of 10 km and 100 km. The direct ICXT level was obtained with Eq. (7), following the directions of signal propagation assigned in Fig. 3. The indirect, Rayleigh backscattered and back-reflected ICXT levels were calculated using Eqs. (8) to (10). The attenuation of the fiber is assumed to be 0.22 dB/km, and the remaining parameters required for the ICXT level calculations and their respective references are presented in Table 2.

From Fig. 8(a), for the square layout, we can see that in bidirectional transmission, the cores most affected by ICXT are the four cores closest to the center, as in unidirectional transmission. However, in bidirectional transmission, this layout leads to a significant reduction of the direct ICXT level, 30 dB lower than the indirect ICXT level, which is the strongest ICXT contribution for this layout, for both link lengths of 10 km and 100 km. This conclusion differs from [27], where the implementation of PDI in a 24-core MCF with the square layout was studied, and the authors claimed that at 100 km the Rayleigh-backscattered ICXT is the most dominant ICXT level in bidirectional transmission. However, this is justified by the fact that in that study, the core pitch of the 24-core MCF is 33.3 μm, due to an increased CD of 250 μm, which leads to a core-to-core direct ICXT level of around -26 dB at 100 km, as opposed to the −11.6 dB at 100 km obtained in the standard CD 12-core MCF with the square layout. As such, at 100 km, for each interfering core, the indirect ICXT level contribution in the 24-core MCF with the square layout is equal to −55 dB, and the Rayleigh backscattered ICXT level contribution is equal to −43 dB, whilst in the standard CD 12-core MCF with the same layout, the indirect ICXT level contribution is equal to −26.2 dB, and the Rayleigh backscattered ICXT level contribution is equal to −26.6 dB. Hence,

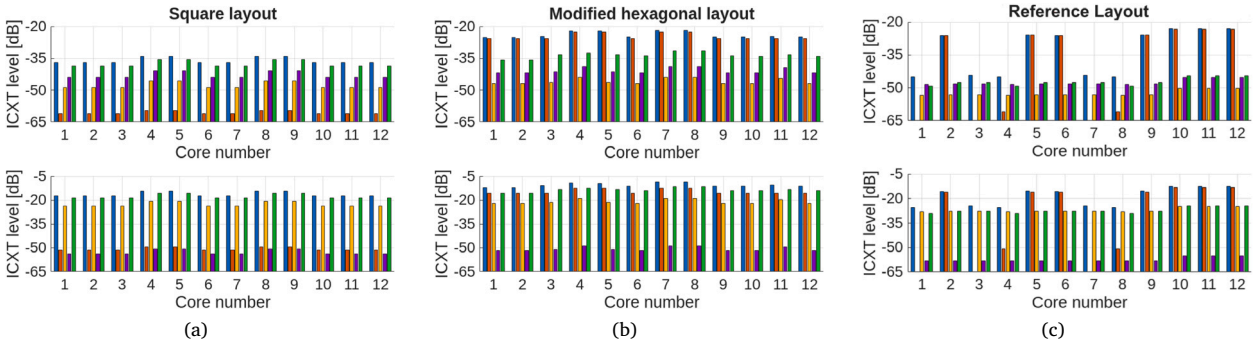


Fig. 8. ICXT level in bidirectional transmission for each core of the (a) square layout, (b) modified hexagonal layout and (c), reference layout for unidirectional transmission. The graphs in the top row are for a fiber length of 10 km, and the bottom row for 100 km. The blue, orange, yellow, purple and green bars represent the bidirectional, direct, Rayleigh backscattered, back-reflected and indirect ICXT levels, respectively.

given that there are twelve contributions to the indirect ICXT level and only four to the Rayleigh backscattered ICXT level in the 12-core square layout with PDI, we can conclude that when the core-to-core direct ICXT level in the square layout is increased, the indirect ICXT level overtakes the Rayleigh backscattered ICXT level as the dominant contribution in bidirectional transmission at 100 km. This conclusion is in agreement with Figure 4 (a) of [25], where Rayleigh backscattered ICXT and indirect ICXT levels are shown as a function of core-to-core direct ICXT level (albeit for a 2-core MCF).

For the case of the modified hexagonal layout, Fig. 8(b), along with cores 4, 7 and 8, core 5 is also one of the most affected cores, due to the fact that with the directions of signal propagation assigned, these four cores now share the same amount of surrounding cores contributing to the direct ICXT level. For this layout, the highest ICXT contribution at 10 km is still the direct ICXT, even when PDI is applied, due to the same direction of signal propagation in some adjacent cores. At a fiber length of 100 km, the indirect ICXT surpasses the direct ICXT as the highest ICXT contribution.

Lastly, Fig. 8(c) shows that the reference layout for unidirectional transmission, when applied to bidirectional transmission, has the direct ICXT as the highest contribution to bidirectional ICXT, due to the fact that PDI cannot be applied to every core pair. As such, the number of adjacent cores with equal directions of signal propagation is only reduced by half, thus reducing the direct ICXT level by only 3 dB. However, it should be noted that due to the increased core pitch and reduced number of adjacent cores when compared to the modified hexagonal layout, this layout has lower ICXT levels for the remaining contributions, and as so achieves a lower total bidirectional ICXT, despite having similar direct ICXT levels.

Similarly to Fig. 7, in Fig. 9 the bidirectional ICXT level and indirect ICXT level of the worst core of each layout are presented as a function of the fiber length. By comparing Figs. 7 and 9, we can conclude that, by employing bidirectional transmission with PDI, all three layouts benefited from an ICXT reduction. For the modified hexagonal layout and reference layout, an ICXT reduction of, respectively, 9 dB and 3 dB is achieved, for fiber lengths shorter than 10 km. For the square layout, the ICXT level reduction obtained is much more substantial, at over 18 dB for fiber lengths shorter than 10 km. As for the indirect ICXT level, whilst the modified hexagonal and the reference layout benefited from a 2 dB and 3 dB reduction, respectively, the same indirect ICXT level was obtained for the square layout in both unidirectional and bidirectional transmission. This is justified by the fact that, when applying PDI as shown in Fig. 3(a), for any interfered core, the adjacent cores have opposite directions of signal propagation, whilst the second adjacent cores maintain the same direction. As such, for the indirect ICXT level, the same number of interfering cores occur in both scenarios. It should also be noted that, for longer lengths, the total ICXT level in the square layout increases faster than in the other

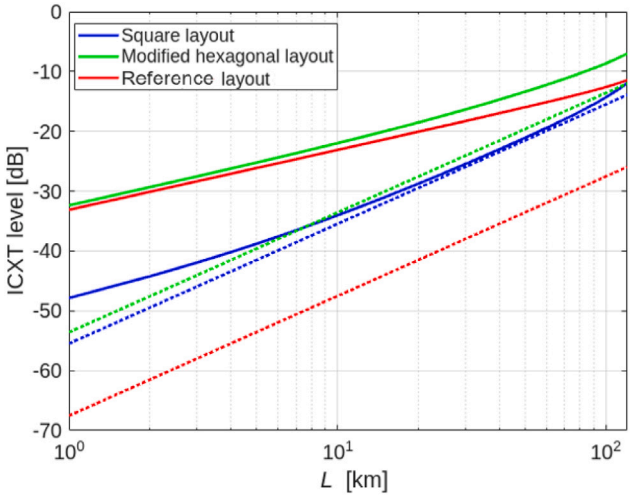


Fig. 9. ICXT level in bidirectional transmission as a function of the fiber length, for the most affected core of the 12-core WC-MCF reference, modified hexagonal and square layouts for a wavelength of 1565 nm. The full and dotted lines represent the total and indirect ICXT levels, respectively.

layouts. To understand why, Fig. 10 shows the individual ICXT level contributions for the worst core of the square layout, for fiber lengths between 1 km and 120 km.

From Fig. 10, we can conclude that up to a 4 km fiber length, the back reflected ICXT is the most predominant contribution to the bidirectional ICXT level, as typically occurs for short-reach links [25]. Beyond this length, due to the decay in the back-reflected ICXT level, and the high number of adjacent and second adjacent cores in combination with a relatively short core pitch, the indirect ICXT level becomes the most prevalent, being responsible for almost all total ICXT level in bidirectional transmission. The fact that, for lengths longer than 4 km, the square layout is most affected by the indirect ICXT, which grows quadratically with link length, justifies the faster bidirectional ICXT level increase when compared to the other two layouts (see Fig. 9), whose main ICXT level contributor is the direct ICXT, which grows linearly with length. For lengths above 40 km, the Rayleigh backscattered ICXT level starts increasing faster than the indirect ICXT level, and has some contribution to the bidirectional ICXT level, for link lengths longer than 100 km. Furthermore, Fig. 10 also shows that the direct ICXT level can be neglected, since the lowest difference to the highest ICXT level contribution at any fiber length is above 20 dB.

The maximum allowed ICXT level of −23.3 dB, established in Section 2.2, for transmission in short-reach links, is marked by the vertical

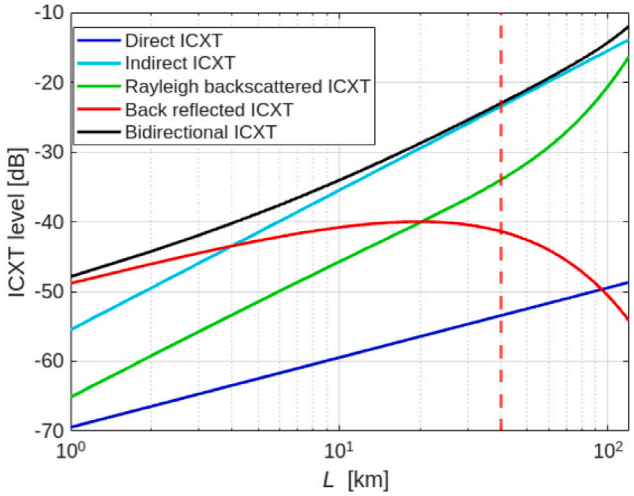


Fig. 10. Bidirectional ICXT level and its contributions as a function of fiber length, for the 12-core square layout represented in Fig. 3(a), for a wavelength of 1565 nm. The vertical dashed red line marks the fiber length where the bidirectional ICXT level reaches −23.3 dB.

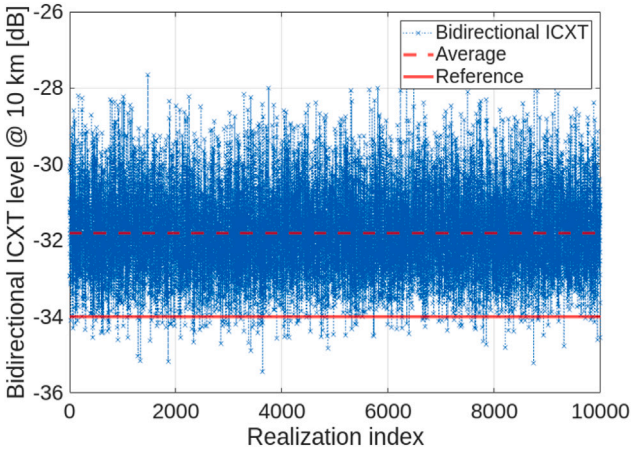


Fig. 11. Bidirectional ICXT level at 10 km obtained for 10000 realizations, for the 12-core square layout, with the same parameters used in Section 4.2, and δC_{max} of 1 μm. The dashed red line represents the average bidirectional ICXT level obtained after averaging the 10000 realizations, and the full red line represents the reference bidirectional ICXT level of the square layout, when δC_{max} is 0 μm.

red dashed line, being achieved at a 37 km length. For lengths of 1 km and 10 km, the 12-core WC-MCF with the square layout achieves a bidirectional ICXT level of −47.8 dB and −34 dB, respectively, showing that this layout is the most suitable for bidirectional short-reach transmission with the use of PDI. At 10 km, the two other fiber layouts have already surpassed the −23.3 dB maximum ICXT level (as shown in Fig. 9).

4.3. Core concentricity error impact on ICXT

In the previous subsection, the ICXT levels of the square layout were obtained assuming that the cores are in the designed position. However, due to inevitable manufacturing errors, the cores in a fabricated MCF may suffer a deviation in their center position. The distance from the center of core n in the design and the center of core n in the fabricated fiber is called core concentricity error, defined as δC_n [10]. To understand how the core concentricity error can affect the ICXT levels of the square layout with the parameters of Section 4.2, a random offset is introduced to the positions of each core. This offset is obtained by:

$$\delta_x = r \cdot \cos(\theta) \tag{18a}$$

$$\delta_y = r \cdot \sin(\theta) \tag{18b}$$

where θ is a random variable corresponding to an angle with uniform distribution between 0 and 2π, and r is a random variable corresponding to a radius with uniform distribution between 0 and δC_{max}, where δC_{max} is the maximum core concentricity error considered.

In [10], the authors measured the core concentricity error of three fabricated 4-core MCFs, and found that the highest error was 1 μm. As such, we will use this value as the worst case of δC_{max}. Fig. 11 shows the bidirectional ICXT level obtained for the 12-core square layout at 10 km, for 10000 realizations, when δC_{max} is set to 1 μm. The average bidirectional ICXT level obtained over 10000 realizations, represented in Fig. 11 by the dashed red line, is −31.8 dB, which represents a 2.2 dB increase from the reference value of −34 dB, the ICXT level with no core concentricity error, marked in the figure by the solid red line. Furthermore, we can see that for a few realizations, the ICXT level obtained was lower than the reference one. This happens because, in this study of the core concentricity error, there is no imposition to ensure that the OCT remains the same, and as such, when the cores are moved outwards, the core pitch is increased at the cost of a lower OCT and higher CL, leading to a decreased ICXT level.

To better understand the influence of the core concentricity error on the square layout, further simulations were made, for δC_{max} of 0.25 μm, 0.5 μm and 0.75 μm, as shown in Fig. 12, where the results for 1 μm are also included. As expected, a lower maximum core concentricity error results in a lower average bidirectional ICXT level. For the maximum core concentricity error of 1 μm, the worst bidirectional ICXT level obtained was −27.5 dB, corresponding to a significant increase of 6.5 dB from the reference value of −34 dB at 10 km. One noteworthy observation is that, whilst the worst bidirectional ICXT level increases over 1 dB with each 0.25 μm increase in δC_{max}, the best bidirectional ICXT level decreases less than 1 dB every 0.25 μm. This can be explained by the fact that, for the ICXT level to decrease significantly, all cores would need to shift away radially from the fiber center, and the probability of all 12 cores moving in that direction is lower than the probability of moving in different directions.

As such, for the maximum core concentricity error, the bidirectional ICXT level of the square layout at a distance of 10 km can suffer an average increase of up to 2.2 dB, with a worst case scenario of 6.5 dB. It should be noted that this error will also have implications on CL and gap between trenches, however, in this work, this impact is not assessed.

5. Conclusions

In this work, four 12-core layouts found in the literature were applied to standard CD WC-MCFs and compared in regard to their geometrical features, ICXT level and suitability for bidirectional transmission with PDI. For a standard CD, with adequate core parameters and OCT, all of the layouts achieve a core pitch considerably shorter than the 30 μm commonly attributed to WC-MCFs, resulting in very short gaps between the trenches, bordering the limits of manufacturing feasibility.

It is confirmed that the reference layout for unidirectional transmission, obtained from the packing circles in circles problem, indeed yields the lowest ICXT level in unidirectional transmission. However, when applied to bidirectional transmission, this layout is incompatible with PDI in all core pairs, and, as such, the direct ICXT level is reduced only by 3 dB.

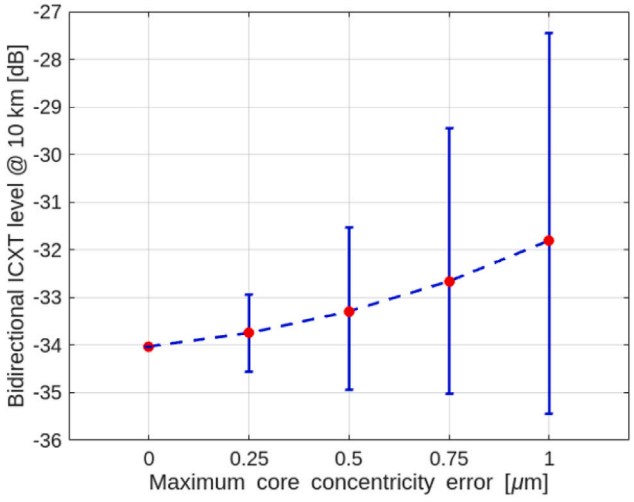


Fig. 12. Bidirectional ICXT level at 10 km obtained for the 12-core square layout, with the same parameters used in Section 4.2, and δC_{max} of 0 μm, 0.25 μm, 0.5 μm, 0.75 μm and 1 μm. The red dots represent the average value for 10000 realizations, with the blue bars marking the lowest and highest values of those 10000 realizations.

With a standard CD, feasible core structure parameters, an OCT of 22.5 μm, a core pitch of 25.3 μm, a gap between trenches larger than 3 μm, operating at the longer wavelength of the C-band, while keeping an acceptable CL of 0.0045 dB/km, the square layout leads to a direct ICXT level of −25.6 dB/km in unidirectional transmission. By employing bidirectional transmission with PDI, a significant total ICXT reduction of more than 18 dB for lengths below 10 km is achieved, resulting in a total bidirectional ICXT level of −47.8 dB and −34 dB at 1 km and 10 km, respectively. Hence, this layout reaches the maximum ICXT level of −23.3 dB allowed for short-reach transmission with 4-PAM at a 37 km length, corresponding to a 35 km longer reach than the one obtained with unidirectional transmission. Furthermore, we conclude that a maximum core concentricity error of 1 μm results in an average 2.2 dB increase in the bidirectional ICXT level at 10 km.

CRediT authorship contribution statement

Tomás I. Martins: Writing – review & editing, Writing – original draft, Visualization, Validation, Software, Methodology, Investigation, Formal analysis. **João L. Rebola:** Writing – review & editing, Validation, Supervision, Resources, Project administration, Methodology, Formal analysis, Conceptualization. **Adolfo V.T. Cartaxo:** Writing – review & editing, Validation, Supervision, Resources, Project administration, Methodology, Formal analysis, Conceptualization.

Declaration of competing interest

The authors declare that they have no known competing financial interests or personal relationships that could have appeared to influence the work reported in this paper.

Acknowledgments

This work was supported in part by LUMIRing, ref. LISBOA2030-FEDER-01319100, which is co-funded by the Lisbon Regional Programme through Portugal 2030 and by the European Union, and is also partially funded by Calouste Gulbenkian Foundation, Portugal. FCT — Fundação para a Ciência e a Tecnologia, I.P., from Portugal, is also acknowledged under projects UID/50008/2025 — Instituto de Telecomunicações and 2023.16564.ICDT.

Data availability

The authors are unable or have chosen not to specify which data has been used.

References

[1] International Telecommunication Union, Measuring Digital Development – Facts and Figures 2023, Tech. rep, ITU, Geneva, Switzerland, 2023.
[2] W. Klaus, P. Winzer, K. Nakajima, The role of parallelism in the evolution of optical fiber communication systems, Proc. IEEE 110 (2022) 1619–1654, http://dx.doi.org/10.1109/JPROC.2022.3207920.
[3] K. Saitoh, Multi-core fiber technology for SDM: Coupling mechanisms and design, J. Lightwave Technol. 40 (2022) 1527–1543, http://dx.doi.org/10.1109/JLT.2022.3145052.
[4] R.-J. Essiambre, G. Kramer, P. Winzer, G. Foschini, B. Goebel, Capacity limits of optical fiber networks, J. Lightwave Technol. 28 (4) (2010) 662–701, http://dx.doi.org/10.1109/JLT.2009.2039464.
[5] G. Saridis, D. Alexandropoulos, G. Zervas, D. Simeonidou, Survey and evaluation of space division multiplexing: From technologies to optical networks, IEEE Commun. Surv. & Tutorials 17 (4) (2015) 2136–2156, http://dx.doi.org/10.1109/COMST.2015.2466458.
[6] T. Hayashi, T. Nakanishi, Multi-core optical fibers for the next-generation communications, SEI Tech. Rev. 86 (2018) 23–28.
[7] M. Koshiba, K. Saitoh, Y. Kokubun, Heterogeneous multi-core fibers: Proposal and design principle, IEICE Electron. Express 6 (2009) 98–103, http://dx.doi.org/10.1587/elex.6.98.
[8] B. Puttnam, R. Luis, E. Agrell, G. Rademacher, J. Sakaguchi, W. Klaus, G. Saridis, Y. Awaji, N. Wada, High capacity transmission systems using homogeneous multi-core fibers, J. Lightwave Technol. 35 (2017) 1157–1167, http://dx.doi.org/10.1109/JLT.2017.2669207.
[9] B.J. Puttnam, R.S. Luís, G. Rademacher, A. Alfredsson, W. Klaus, J. Sakaguchi, N. Wada, Characteristics of homogeneous multi-core fibers for SDM transmission, APL Photonics 4 (2) (2019) 022804, http://dx.doi.org/10.1063/1.5048537.
[10] T. Mori, Y. Yamada, K. Shibahara, T. Matsui, M. Kikuchi, Y. Sagae, D. Soma, S. Beppu, T. Nagashima, T. Morishima, T. Hayashi, M. Ohzeki, K. Takenaga, M. Takahashi, T. Sasaki, R. Sugizaki, Y. Miyamoto, K. Nakajima, Applicability of standard cladding diameter multi-core fiber cables for terrestrial field, J. Lightwave Technol. 42 (2024) 1044–1055, http://dx.doi.org/10.1109/JLT.2023.3333429.
[11] L. Gan, J. Zhou, S. Fu, M. Tang, D. Liu, Efficient channel model for homogeneous weakly coupled multicore fibers, IEEE J. Sel. Top. Quantum Electron. 26 (2020) http://dx.doi.org/10.1109/JSTQE.2019.2916423.
[12] T. Matsui, P. Pondillo, K. Nakajima, Weakly coupled multicore fiber technology, deployment, and systems, Proc. IEEE 110 (2022) 1772–1785, http://dx.doi.org/10.1109/JPROC.2022.3202812.
[13] R. Luís, B. Puttnam, G. Rademacher, W. Klaus, E. Agrell, Y. Awaji, N. Wada, On the spectral efficiency limits of crosstalk-limited homogeneous single-mode multi-core fiber systems, in: Advanced Photonics 2017, OSA, 2017, p. NeTu2B.2, http://dx.doi.org/10.1364/NETWORKS.2017.NeTu2B.2.
[14] R.S. Luis, B.J. Puttnam, G. Rademacher, S. Shinada, T. Hayashi, T. Nakanishi, Y. Saito, T. Morishima, H. Furukawa, 12.8 Tb/s SDM optical interconnect for a spine-leaf datacenter network with spatial channel connectivity, in: 2022 European Conference on Optical Communication, ECOC, 2022.
[15] R. Dias, J. Rebola, A. Cartaxo, Outage probability due to crosstalk from multiple interfering cores in PAM4 inter-datacenter connections, Photonics 8 (1) (2021) 9, http://dx.doi.org/10.3390/photonics8010009.
[16] D. Soma, S. Beppu, Y. Miyagawa, N. Yoshikane, T. Tsuritani, 114 Pbit/s·km transmission using three vendor-installed 60-km standard cladding multi-core fiber spans with multiple fusion splicing, in: 2023 Optical Fiber Communications Conference and Exhibition, OFC, 2023, pp. 1–3, http://dx.doi.org/10.1364/OFC.2023.Tu2C.5.
[17] Y. Chen, Y. Xiao, S. Chen, F. Xie, Z. Liu, D. Wang, X. Yi, C. Lu, Z. Li, Field trials of communication and sensing system in space division multiplexing optical fiber cable, IEEE Commun. Mag. 61 (8) (2023) 182–188, http://dx.doi.org/10.1109/MCOM.004.2200885.
[18] Sumitomo Electric Industries, Ltd., The world's first field deployed multi-core fiber testbed for optical communications installed in L'Aquila, Italy, 2019, https://global-sei.com/company/press/2019/06/prs043.html. (Accessed October 2025).
[19] LUMIRing: Lisbon underground multicore fiber ring project, 2025, https://lumiring.iscte-iul.pt/. (Accessed October 2025).
[20] Google Cloud, delivering multi-core fiber technology in subsea cables, 2023, Google Cloud Blog. (Accessed October 2025).
[21] T. Matsui, T. Sakamoto, Y. Goto, K. Saito, K. Nakajima, F. Yamamoto, T. Kurashima, Design of 125 μm cladding multi-core fiber with full-band compatibility to conventional single-mode fiber, in: 2015 European Conference on Optical Communication, ECOC, IEEE, 2015, http://dx.doi.org/10.1109/ECOC.2015.7341966.

[22] T. Matsui, Y. Sagae, T. Sakamoto, K. Nakajima, Design and applicability of multi-core fibers with standard cladding diameter, J. Lightwave Technol. 38 (2020) 6065–6070, http://dx.doi.org/10.1109/JLT.2020.3004824.
[23] T. Hayashi, T. Nakanishi, K. Hirashima, O. Shimakawa, F. Sato, K. Koyama, A. Furuya, Y. Murakami, T. Sasaki, 125 μm cladding eight-core multi-core fiber realizing ultra-high-density cable suitable for O-band short-reach optical interconnects, J. Lightwave Technol. 34 (2016) 85–92, http://dx.doi.org/10.1109/JLT.2015.2470078.
[24] F. Zhang, C. Yang, Z. Song, H. Du, Z. Liu, J. Tang, Y. Meng, M. Tang, Design and fabrication of 125 μm standard cladding diameter heterogeneous 8-core fiber with ultra-low crosstalk for C-band transmission, J. Lightwave Technol. 42 (2024) 5681–5690, http://dx.doi.org/10.1109/JLT.2024.3398785.
[25] T. Hayashi, T. Nagashima, A. Inoue, H. Sakuma, T. Suganuma, T. Hasegawa, Uncoupled multi-core fiber design for practical bidirectional optical communications, in: Optical Fiber Communications Conference and Exhibition (OFC), OFC, 2022.
[26] A. Sano, H. Takara, T. Kobayashi, Y. Miyamoto, Crosstalk-managed high capacity long haul multicore fiber transmission with propagation-direction interleaving, J. Lightwave Technol. 32 (2014) 2771–2779, http://dx.doi.org/10.1109/JLT.2014.2320826.
[27] F. Ye, J. Tu, K. Saitoh, K. Takenaga, S. Matsuo, H. Takara, T. Morioka, Design of homogeneous trench-assisted multi-core fibers based on analytical model, J. Lightwave Technol. 34 (18) (2016) 4406–4416, http://dx.doi.org/10.1109/JLT.2016.2599187.
[28] A. Sano, H. Takara, T. Kobayashi, H. Kawakami, H. Kishikawa, T. Nakagawa, Y. Miyamoto, Y. Abe, H. Ono, K. Shikama, M. Nagatani, T. Mori, Y. Sasaki, I. Ishida, K. Takenaga, S. Matsuo, K. Saitoh, M. Koshiba, M. Yamada, H. Masuda, T. Morioka, 409-Tb/s + 409-Tb/s crosstalk suppressed bidirectional MCF transmission over 450 km using propagation-direction interleaving, Opt. Express 21 (14) (2013) 16777–16783, http://dx.doi.org/10.1364/OE.21.016777, URL https://opg.optica.org/oe/abstract.cfm?URI=oe-21-14-16777.
[29] O. Ozolins, J.M. Estaran, A. Udalcovs, F. Jorge, H. Mardoyan, A. Konczykowska, M. Riet, B. Duval, V. Nodjiadjim, J.-Y. Dupuy, X. Pang, U. Westergren, J. Chen, S. Popov, S. Bigo, 140 Gbaud on-off keying links in C-band for short-reach optical interconnects, in: 2018 European Conference on Optical Communication, ECOC, 2018, http://dx.doi.org/10.1109/ECOC.2018.8535208.
[30] T. Hayashi, Multi-core fiber technology from design to deployment, in: 2022 European Conference on Optical Communication, ECOC, 2022.
[31] F. Ye, J. Tu, K. Saitoh, T. Morioka, Simple analytical expression for crosstalk estimation in homogeneous trench-assisted multi-core fibers, Opt. Express 22 (2014) 23007, http://dx.doi.org/10.1364/oe.22.023007.
[32] J. Tu, K. Saitoh, M. Koshiba, K. Takenaga, S. Matsuo, Design and analysis of large-effective-area heterogeneous trench-assisted multi-core fiber, Opt. Express 20 (2012) 15157, http://dx.doi.org/10.1364/OE.20.015157.
[33] T. Hayashi, T. Sakamoto, Y. Yamada, R. Ryf, R.-J. Essiambre, N. Fontaine, M. Mazur, H. Chen, T. Hasegawa, Randomly-coupled multi-core fiber technology, Proc. IEEE 110 (2022) 1786–1803, http://dx.doi.org/10.1109/JPROC.2022.3182049.
[34] A. Cartaxo, Loss imbalance effect on inter-core crosstalk in bidirectional uncoupled multi-core fiber transmission, J. Lightwave Technol. 41 (2023) 5911–5921, http://dx.doi.org/10.1109/JLT.2023.3273233.
[35] T. Hayashi, A. Inoue, Y. Suzuki, Y. Norisugi, K. Kawamoto, J. Takano, T. Nagashima, T. Hirama, K. Takeda, Y. Shimoda, F. Sato, Ultra-high-density microduct cable with uncoupled 12-core fibers with standard 250 μm coating, in: Optical Fiber Communication Conference, 2023, http://dx.doi.org/10.1364/OFC.2023.Tu2C.2, URL https://opg.optica.org/abstract.cfm?URI=OFC-2023-Tu2C.2.
[36] T. Gonda, K. Imamura, R. Sugizaki, Multicore fiber for bi-directional transmission, in: 2016 21st OptoElectronics and Communications Conference (OECC) Held Jointly with 2016 International Conference on Photonics in Switching, PS, 2016.
[37] Y. Seki, Y. Tanigawa, Y. Hirota, H. Tode, Which multi-core fiber layout is best for highest capacity network design? in: 49th European Conference on Optical Communications (ECOC 2023), 2023, pp. 365–368, http://dx.doi.org/10.1049/icp.2023.2081.
[38] Y. Goto, K. Nakajima, T. Matsui, T. Kurashima, F. Yamamoto, Influence of cladding thickness on transmission loss and its relationship with multicore fiber structure, J. Lightwave Technol. 33 (23) (2015) 4942–4949, http://dx.doi.org/10.1109/JLT.2015.2493372.
[39] E. Specht, Packomania, 2025, www.packomania.com. (Accessed October 2025).
[40] Y. Tobita, T. Fujisawa, T. Sakamoto, T. Matsui, S. Saitoh, K. Takenaga, K. Aikawa, S. Aozasa, K. Nakajima, K. Saitoh, Optimal design of 4LP-mode multicore fibers for high spatial multiplicity, Opt. Express 25 (5) (2017) 5697, http://dx.doi.org/10.1364/OE.25.005697.
[41] K. Saitoh, S. Matsuo, Multicore fiber technology, J. Lightwave Technol. 34 (2016) 55–66, http://dx.doi.org/10.1109/JLT.2015.2466444.
[42] R. Kingsta, R. Selvakumari, A review on coupled and uncoupled multicore fibers for future ultra-high capacity optical communication, Optik 199 (2019) http://dx.doi.org/10.1016/j.ijleo.2019.163341.
[43] X. Mu, A. Ottino, F.M. Ferreira, G. Zervas, Design and transmission analysis of trench-assisted multi-core fibre in standard cladding diameter, Opt. Express 30 (21) (2022) 38152–38166, http://dx.doi.org/10.1364/OE.472430.
[44] T. Hayashi, Accuracy of analytical expressions for Rayleigh backscattered crosstalk in bidirectional multi-core fiber transmissions, Opt. Express 30 (2022) 23943, http://dx.doi.org/10.1364/oe.460565.